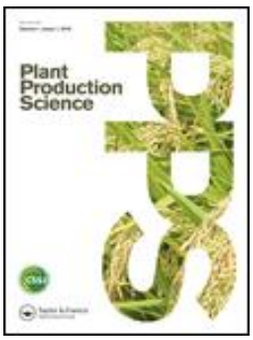

Plant Production Science

ISSN: (Print) (Online) Journal homepage: https://www.tandfonline.com/loi/tpps20

Field phenotyping of plant height in an upland rice field in Laos using low-cost small unmanned aerial vehicles (UAVs)

Kensuke Kawamura , Hidetoshi Asai , Taisuke Yasuda , Phanthasin Khanthavong , Pheunphit Soisouvanh & Sengthong Phongchanmixay

To cite this article: Kensuke Kawamura , Hidetoshi Asai , Taisuke Yasuda , Phanthasin Khanthavong , Pheunphit Soisouvanh & Sengthong Phongchanmixay (2020): Field phenotyping of plant height in an upland rice field in Laos using low-cost small unmanned aerial vehicles (UAVs), Plant Production Science, DOI: 10.1080/1343943X.2020.1766362

To link to this article: https://doi.org/10.1080/1343943X.2020.1766362

Published online: 01 Jun 2020.

PLANT PRODUCTION SCIENCE
https://doi.org/10.1080/1343943X.2020.1766362

REGULAR PAPER

OPEN ACCESS Check for updates

Field phenotyping of plant height in an upland rice field in Laos using low-cost small unmanned aerial vehicles (UAVs)

Kensuke Kawamura[a*], Hidetoshi Asai[a*], Taisuke Yasuda[b], Phanthasin Khanthavong[c], Pheunphit Soisouvanh[d] and Sengthong Phongchanmixay[d]

[a]Japan International Research Center for Agricultural Sciences (JIRCAS), Tsukuba, Japan; [b]Mount Fuji Research Institute, Yamanashi Prefectural Government, Fujiyoshida, Japan; [c]Maize and Cash Crops Research Center, National Agriculture and Forestry Research Institute (NAFRI), Vientiane, Laos; [d]Rice Research Center, National Agriculture and Forestry Research Institute (NAFRI), Vientiane, Laos

ABSTRACT

Plant height (PH) is an important agronomical parameter to assess the growth status in upland rice fields. Recently, field-based phenotyping using unmanned aerial vehicles (UAVs) has received increasing attention as a cost-effective, well-suited sensing technology to measure PH. In this study, we evaluated feasibility of a low-cost small UAV for estimating PH in upland rice fields in Laos with a canopy height model (CHM). Images of the upland field, including 501 plots (= 167 accessions × 3 replicates), were captured by a commercial small UAV (DJI Phantom 4) before emergence and in the near-flowering stage to generate digital surface models (DSMs). The CHM was developed from the difference of the DSMs using UAV images obtained before emergence and before flowering. The CHM metrics of each plot were then calculated using 90–99th percentiles and the top 1–10% largest pixel values of CHM and were compared with the manually measured field PH (78.25–189.75 cm). The predictive accuracy was assessed in the 90–99th percentiles and top 1–10% values of CHM metrics with 5-fold cross-validation procedures. Simple linear regression analyses between the field PH and CHM metrics showed that the top 3% CHM metrics had the best correlation with the field PH (R^2 = 0.712, root-mean-square error (RMSE) = 9.142 cm, $p < 0.001$). Cross-validation procedures also confirmed that the top 3% CHM metrics were the best in terms of accuracy for estimating PH, with an error of 6.963% (8.823 cm) error.

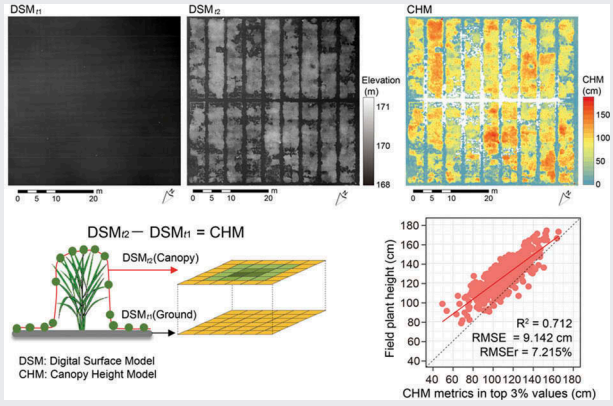

ARTICLE HISTORY
Received 13 October 2019
Revised 6 April 2020
Accepted 27 April 2020

KEYWORDS
Canopy height model; digital surface model; phenotyping; structure from motion; UAV; upland rice

1. Introduction

Upland rice grown in unbundled fields without water flooding is still a dominant crop in developing countries, where irrigation facilities are poorly equipped (Saito et al., 2018). In the Lao People's Democratic Republic (hereafter, Laos), upland subsistence farmers crop rice on sloping land with crop-fallow rotational management. The ethnic and environmental diversity together with the fact that Laos is a neighboring area of rice origin result in the formation of rich genotypic diversity in upland rice ecosystems (Appa Rao et al., 2006). However, the yield level is generally low (approximately, 2.0 t ha^{-1}) due to the erratic rainfall pattern and soil nutrient depletion, and it has been generally stagnant over the past two decades (Asai et al., 2017; Asai et al., 2009). To overcome the yield barrier, the development

CONTACT Kensuke Kawamura kamuken@affrc.go.jp; Hidetoshi Asai asai0817@affrc.go.jp

*These authors contributed equally to this work.

of new varieties that can adapt to stress conditions could represent a key approach and the existing genotypic diversity could provide promising materials for breeding. However, these local resources have been rarely evaluated and never used for breeding because phenotyping is a time-consuming process that often represents a constraint due to the limitation of financial and human-resource capacities. Therefore, high-throughput strategies in the phenotyping process are necessary requirement to maximize the potential of local genotypic resources.

In crop phenotyping, plant height (PH) is a basic agronomical parameter for field investigation, and widely used to assess the aboveground biomass and potential grain yield (Boomsma et al., 2010; Salas Fernandez et al., 2009). Traditionally, the crop PH is manually measured using a ruler in the field by selecting a few plants per plot (usually 1 to 2 m^2) to represent the canopy status. However, manual PH measurements in the field are labor-intensive for large-scale multi-variety trials and can be limited by bad weather and access to plots over a large area. Therefore, several high-throughput technologies have been developed to retrieve the PH and three-dimensional (3D) structures under field conditions (Sankaran et al., 2015).

High-throughput phenotyping systems require the ability to non-destructively and noninvasively characterize phenotypic traits for thousands of individual plants with high efficiency and precision (Furbank & Tester, 2011; Großkinsky et al., 2015) and to monitor the same plot throughout the whole lifecycle to increase the experimental capacity (Fahlgren et al., 2015). Data acquisition at very high temporal resolution (daily) is essential for certain phenological stages (e.g. heading, emergence, etc.) and the evaluation and selection of the best-performing cultivars (Andrade-Sanchez et al., 2013). For such work, satellites are limited by their overpass frequency and spatial resolution (>50 cm), which does not correlate well with single rice plants. Because rice plants are usually sown in a grid of 20–25 cm intervals, identifying single rice plants is not feasible. Similarly, ground-based sensing platforms are not easily transported from one location to another, surface maps may not be generated in real time, and plant parameters of several plots cannot be measured simultaneously (Sankaran et al., 2015).

Detailed three-dimensional (3D) information on the plant canopy can be obtained via laser scanning techniques, such as airborne light detection and ranging (LiDAR) (Korhonen et al., 2011) and terrestrial laser scanning (TLS) (Côté et al., 2009; Eitel et al., 2014; Hoffmeister et al., 2016). TLS is a ground-based laser scanning technique used to measure the position and dimension of objects in 3D space. Using TLS, Zhang and Grift (2012) developed a stem height measurement system for the bioenergy crop *Miscanthus giganteus*, and it presented an error of 3.8%. W. Zhang et al. (2019) developed a segment-based method for efficient stem detection at the plot level with >95% accuracy. Despite their precision, LiDAR and TLS are not widely available in crop fields due to the payload limitations of small unmanned aerial vehicles (UAVs) and the high relative expense of such vehicles.

Currently, a large number of studies are underway to realize field-based phenotyping by utilizing UAVs. Small UAVs with suitable sensors (e.g. multi-spectral or hyperspectral camera, thermal camera) for remote sensing of plant responses (to induced abiotic and biotic stress) and performance (yield) under field conditions have several benefits. The integrated system can provide (i) better access to the field, (ii) high-resolution data (1–2 cm depending on the flying altitude), (iii) timely data collection (even under cloudy conditions), (iv) quick field growth evaluations, (v) simultaneous image acquisition, (vi) self-automated flights for monitoring the plots at regular periods in a given growing season, and (vii) low operational costs compared to other low-altitude platforms (e.g. airborne, balloon, etc.; Araus & Cairns, 2014; Berni et al., 2009; Hunt et al., 2010; Nebiker et al., 2008; Zhang & Kovacs, 2012).

To date, the feasibility of UAV platforms for estimating PH and 3D structure has been demonstrated in barley (Bendig et al., 2013, 2014, 2015), maize (Li et al., 2016; Wang et al., 2019), sugarcane (De Souza et al., 2017) and sorghum (Han, Thomasson, Bagnall, Rooney et al., 2018; Hu et al., 2018; Watanabe et al., 2017). Compared with such tall crops (~3.2 m), fewer studies have been conducted on short (~1.2 m) crops such as grassland (Rueda-Ayala et al., 2019; H. Zhang et al., 2018), paddy fields (Stavrakoudis et al., 2019) and wheat (Holman et al., 2016), because of the small variation in PH, thus suggesting lower accuracy. This study conducted in an upland rice field as just a case study on short crops.

In this study, we aimed to evaluate the feasibility of small UAV for estimating PH in multi-variety trials in Laos, which compared the local genetic resource of upland rice, using a canopy height model (CHM). The CHM is a methodology designed to extract the vegetation canopy height parameter from point clouds or digital surface models (DSMs). To extract the CHM linked to the referenced field PH, CHM metrics from the 95th and/or 99th percentiles have widely been used as a better approach to isolate the top photosynthetic tissue of each plant rather than the standard mean or median (Holman et al., 2016; Madec et al., 2017; Watanabe et al., 2017). However, these estimations were based on

the average PH of whole canopy in a plot, which included the heights of lower leaves and even the elevation of bare ground patches within canopy gaps (Bendig et al., 2015). The proportion of the lower layer pixels may increase due to differences in plant structure depending on the successions of rice. Ideally, the CHM metrics generated from the top few percent of pixels may reflect PH more accurately. In this study, CHM metrics from the top 1–10% of the largest pixel values and CHM metrics from the 90–99th percentiles were calculated to estimate the field PH and compare the predictive accuracies.

2. Materials and methods

2.1. Experimental site and field design

Laos is a country that contains one of the largest genetic resources of upland rice in the world (Rao et al., 2006). This study was conducted in an experimental field at the Rice Research Center (RRC) of the National Agriculture and Forestry Research Institute (NAFRI) (18°8′56.65″N, 102°44′9.78″E), in the central part of Vientiane in Laos (Figure 1). This area has a hot, humid summer season and belongs to a tropical climate ('Aw' in Köppen's climate classification). The mean annual temperature is 25.4°C, and the annual precipitation is 1622 mm. The soil type is characterized by clay loam (CL, 0–30 cm) and light clay (LiC, 40–60 cm).

In the rainy season (May to October) of 2018, a field trial was installed for genotypic evaluation of traditional upland rice germplasms of Laos. In total, 167 accessions were collected in Laos, which were selected from a preliminary survey to maximize the phenotypic variations. These germplasms included diverse genotypic backgrounds of *indica* and tropical *japonica* with glutinous and nonglutinous quality. The plots, with a size of 2.0 m × 1.5 m, were laid out in a randomized complete block design with three replications in the experimental field (44 m × 43 m = 1,892 m^2) (Figure 2). Thus, the experimental field contained a total of 501 plots (= 167 accessions × 3 replicates). On 9 June 2018, 5–10 seeds were sown with a dibbling stick at a spacing of 25 cm × 25 cm. Rice was grown under rainfed upland conditions without the addition of water and fertilizer. Before experimental installation, the field was fallow for 2 years. Field preparation was performed with hallow plowing 1 week prior to sowing. Missing hills that did not germinate were replaced 2 weeks after sowing.

The system used in field-based phenotyping should be easier to use and cost-effective. Therefore, small UAVs with an optical camera have been increasingly used to estimate the PH and canopy structure using a combination of the structure from motion (SfM) algorithm and CHM. The SfM is a computer technique that can generate 3D geometries by automatically extracting the corresponding feature points from unordered, overlapped multi-view stereo UAV-based RGB (red-green-blue) images and optimizing the 3D location of corresponding features based on the

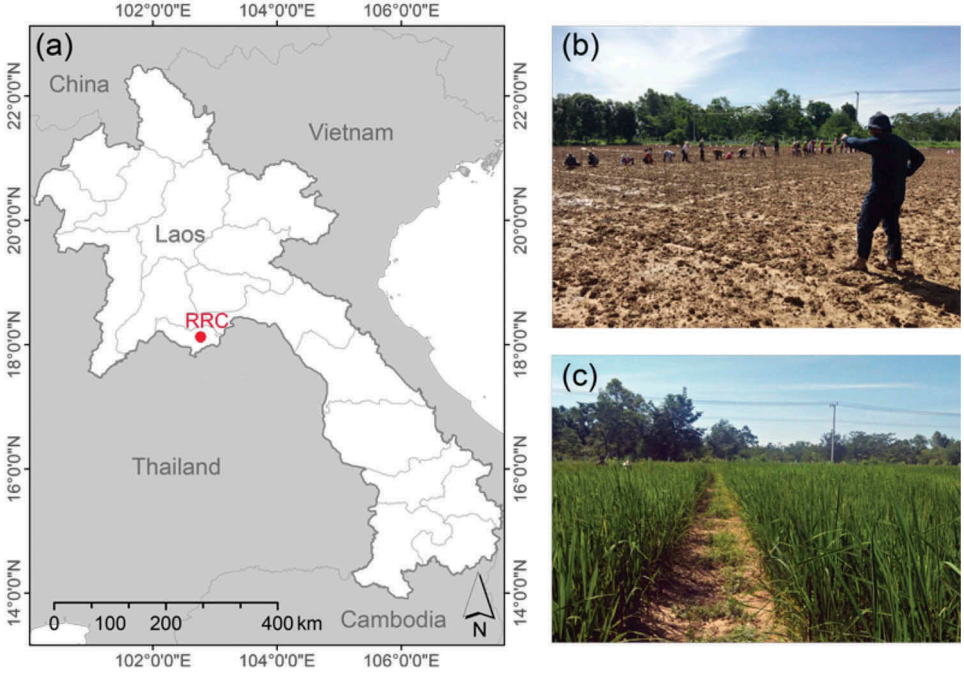

Figure 1. Location of the rice research center (RRC) (a); and the photographs for seeding date (8 June 2018) (b) and before the flowering season (6 September 2018) (c).

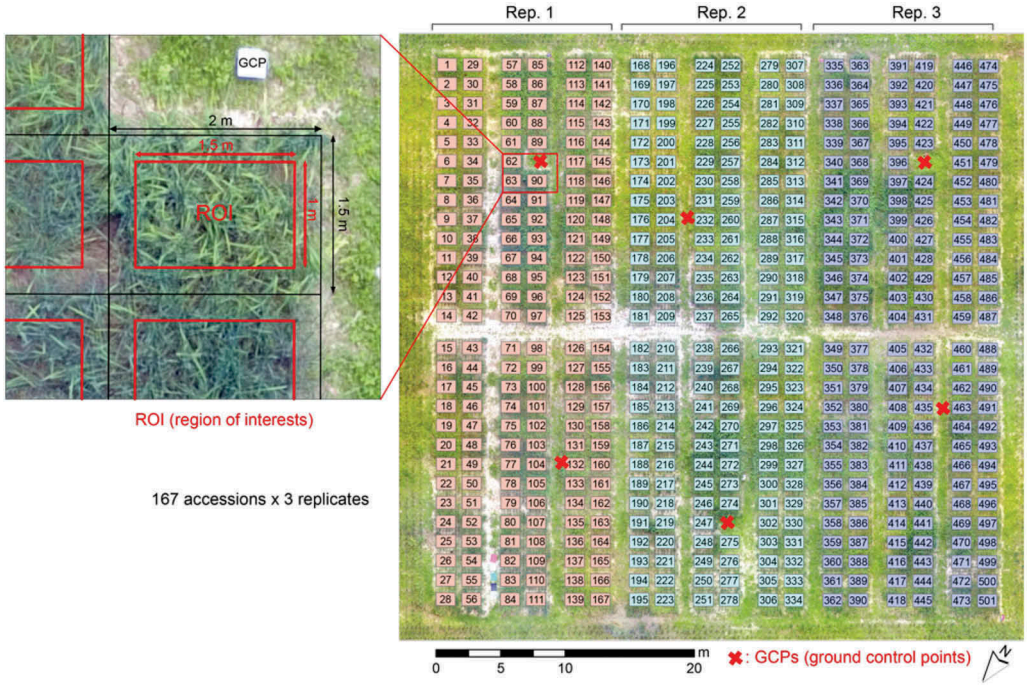

Figure 2. Plot design (167 accessions × 3 replicates, $n = 501$) and plot blocks and region of interest (ROI) in UAV image processing.

principles of photogrammetry (Snavely et al., 2008; Westoby et al., 2012). Using DSMs, the CHM can be computed from the distance between the DSM at ground level and the DSM of the vegetation (Van Iersel et al., 2018). The lower boundary of the DSM at ground level can be easily determined by drone flights at either the pre-sowing stage or early in the season before emergence (Bendig et al., 2013; Holman et al., 2016). Such a raster-based CHM is more precisely 2.5-dimensional (2.5D) because only one z value is stored per x/y coordinate pair (Brocks et al., 2016), and it continuously covers a whole crop stand. The height of an individual plant in the field is of high value for agricultural research.

The field PH, which is referred to as the ground-truth height (cm) from the ground to the apex (highest point), differs depending on the plant growth stage, such as a leaf in the vegetative stage or an ear in a mature stage (Han, Thomasson, Bagnall, Pugh et al., 2018). In the present study, the field PH before flowering was measured weekly over the period from 28 days after sowing (DAS; 29 June 2018) to 110 DAS (19 September 2018) at the rice apices on flag leaf. For prevention of intentional selection, four plants were selected at a fixed hill position for every time of the measurements. Plant growth is expected to peak and PH variations will likely occur due to successions; thus, PH data obtained before flowering on 5 September 2018 (88 DAS) from a total of 501 plots were provided for a coupling analysis with the UAV images taken 3 days after the measurement (8 September 2018; 91 DAS).

2.2. Overview of the methodology

In this section, an overview of the research process is described using a flowchart in Figure 3 that summarizes four steps: (1) acquire RGB images using a small UAV in two seasons (before emergence (RGBt_1) and near the peak growth stage (RGBt_2)); (2) generate dense point clouds and DSMs from RGBt_1 and RGBt_2; (3) calculate the CHM from the distance between DSMt_2 and DSMt_1;

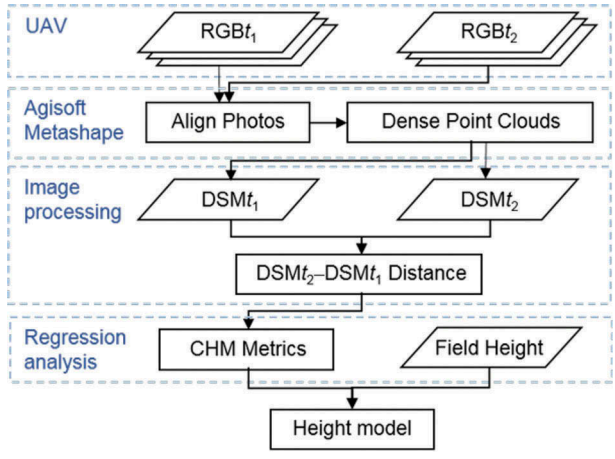

Figure 3. Flowchart depicting a general overview of the methodology.

and (4) develop a PH estimation model. More detailed information is described in the following sections.

UAV image acquisition in step 1 was conducted using a DJI Phantom 4 (DJI, Shenzhen, China) and its 12.4 megapixels standard integrated sensor (4000 × 3000 pixels) was fitted to a 3-axis stabilized gimbal to maintain a fixed viewing angle. The UAV flight operation was performed using Pix4Dcapture version 4.5.0 (Pix4D S.A., Lausanne, Switzerland). Dense point clouds and DSM generation in step 2 were performed using Agisoft Metashape version 1.5.1 (Agisoft LLC, St. Petersburg, Russia). Image processing and regression analysis in steps 3–4 were performed using the statistical software R version 3.5.1 (R Core Team, 2018).

2.3. UAV-RGB image acquisition

A small consumer UAV, the DJI Phantom 4 (DJI, Shenzhen, China), was used to capture the RGB images after seeding (12 June 2018, DAS = 3) and before the flowering stage (8 September 2018, DAS = 91). The UAV flights followed an autonomous flight plan using the 'double grid' mission in Pix4Dcapture (https://support.pix4d.com/hc/en-us/articles/115002496206) (Figure 4) to ensure substantial overlap (i.e. 90% forward and 70% side), and the flight height was 20 m. The camera angle was set at 80° because a previous literature reported that SfM-based DSMs (or digital elevation models (DEMs)) derived from UAV images showed systematic broad-scale deformations, which are expressed as a central 'doming' (Rosnell & Honkavaara, 2012), and the systematic error could be reduced through the collection of oblique imagery (James & Robson, 2014).

For this trial and UAV, the total flight time was approximately 12 min to cover the whole field. Six ground-control points (GCPs) were permanently set up during the trial (Figure 2). In this study, five wooden boards (30 cm × 30 cm) that were painted black or white were used as GCPs. Their positions were measured and recorded using a Trimble Geo 7X GPS (http://www.trimble.com).

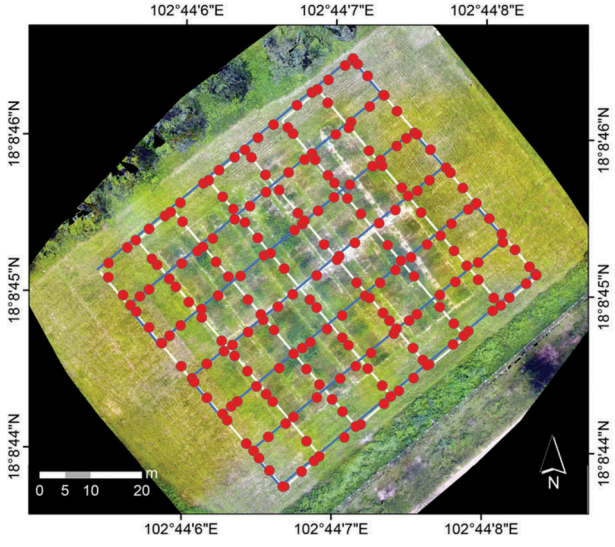

Figure 4. UAV flight trajectory of the flight mode. The solid red dots are the locations of aerial photographs. The pink and white lines are the flight trajectory of the UAV.

2.4. Dense point cloud and DSM generation

Using the commercial SfM software Metashape Pro ver.1.5.1 (Agisoft LLC, St. Petersburg, Russia), the 3D point clouds, ortho-mosaic images and DSMs were constructed from images taken by the UAV with the geographic coordinates of six GCPs (UTM 48 N). The parameter settings used for Agisoft Metashape software are summarized in Table 1.

The accuracy of PH estimation from a CHM is closely related to the upper boundary of generated point-cloud or DSM values. When the quality of the generated point cloud or DSM data is insufficient for distinguishing the ground (lower boundary) and vegetation (upper boundary), the CHM cannot accurately represent the PH information. To achieve the best accuracy in the data set, we set the 'Highest' accuracy in 'Camera alignment' and the 'Ultra high' quality in the 'Build point cloud' processes. In the 'Build point clouds' process, 'Mild depth filtering' was used to achieve greater CHM accuracy (Holman et al., 2016).

The DSMs at ground level (DSMt_1) and canopy level (DSMt_2) were generated with RGB images on 12 June 2018 (before emergence (RGBt_1)) and

Table 1. Parameters of the drone flights and image processing by Metashape Pro software.

Process	Parameter	Setting
Drone flight	Altitude (m)	20 m
	Overlaps	Forward 90% and Side 70%
	Number of GCPs	6
	Coordinate system	WGS 84/UTM 48 N
Camera alignment	Accuracy	Highest
	Adaptive camera model fitting	Yes
Build point clouds	Quality	Ultra high
	Depth filtering	Mild
Build texture	Mapping mode	Adaptive ortho-photo
	Blending mode	Mosaic
Build tile model	Source data	Dense cloud
	Tile size	2048
DSM	Source data	Dense cloud
	Interpolation	Enabled
Orthomosaic	Blending mode	Mosaic
	Surface	DSM

8 September 2018 (near the peak growth stage (RGBt_2)). The ground sample distance (GSD) and pixel size for DSMt_1 and DSMt_2 were approximately 0.93 and 0.88 cm pixel^{-1}, respectively. To simplify for further analyses, the DSMs were exported as GeoTiff format image files with 1 cm GSD.

2.5. CHM and CHM metrics

Based on R software version 3.5.1 (R Core Team, 2018), the DSM Geotiff images were imported, and then DSMt_2 was resampled to fit the pixels with DSMt_1 using the nearest-neighbor method based on the 'resample' function in the 'raster' package version 2.9–5 (Hijmans, 2019). The CHM was generated by computing the distances between DSMt_1 and DSMt_2 as follows:

$$\mathrm{CHM} = \mathrm{DSMt_2} - \mathrm{DSMt_1} \tag{1}$$

Because adjacent plots in the experimental field were close to each other, the CHMs of plot boundaries were considered to be contaminated with data originating from adjacent plots and might have larger error than those inside a plot. To exclude the marginal areas, regions of interest (ROIs) (1.0 m × 1.5 m) were set inside the plot block (1.5 m × 2.0 m), as shown in Figure 2, and the pixel values in ROIs were extracted as CHM metrics. Here, we calculated two types of CHM metric values: 90–99th percentiles (CHM90th to CHM99th) and top 1–10% values (CHM1% to CHM10%) in ROIs as the representative values of CHM metrics for the plot height.

2.6. Statistical analysis

An analysis of variation (ANOVA) for PH was conducted on the data set obtained from 501 plots (167 accessions × 3 replications) using JMP software version 14 (SAS Institute Inc., Cary, NC, 1989–2019). In this analysis, we considered the effects of accession and replication to be fixed. Contribution ratios (%) were estimated for effects of accession and replication by using Equation (2), respectively. Then, contribution ratio for error term was calculated by subtracting the ratios of accession and replication from 100%.

$$P_x = \frac{S_x - \Phi_x \times V_e}{S_t} \tag{2}$$

where P_x, S_x and Φ_x are contribution ratio, sum of square and degree of freedom for the effect of x. The terms of Ve and S_t represent the variance (mean square) of error term and total sum of square.

The relationship between the CHM metrics and field PH was assessed by simple linear regression analysis using R software version 3.5.1 (R Core Team, 2018). The relationships were evaluated by the coefficient of determination (R^2), root mean squared difference (RMSE) and relative RMSE (RMSEr).

$$R^2 = 1 - \frac{\sum_{i-1}^{n} (y_i - \hat{y}_i)^2}{\sum_{i-1}^{n} (y_i - \bar{y}_i)^2} \tag{3}$$

$$\mathrm{RMSEr} = \sqrt{1/n \sum_{i-1}^{n} (y_i - \hat{y}_i)^2} \tag{4}$$

$$\mathrm{RMSEr} = \sqrt{\frac{1/n \sum_{i-1}^{n} (y_i - \hat{y}_i)^2}{\bar{y}} \times 100} \tag{5}$$

where x_i and y_i represent the explanatory variable (CHM) and response variable (field PH) for the ith sample, $\hat{y}_i$ is the predicted values, $\bar{y}$ is the mean of the observed values, and n is the number of samples (plots) in the data set.

To evaluate the predictive ability of CHM metrics, a k-fold cross-validation procedure based on independent training and test data sets was performed (Emmert-Streib & Dehmer, 2019). Initially, the data were divided randomly into training (n = 400) and test (n = 101) data sets. Next, the training data were split randomly into k-folds. Here, we used k = 5; therefore, each k-hold has n = 80 samples. A linear regression model was built on k – 1 folds of training data set (n = 320), and then the error of the kth fold was recorded as validation data (n = 80). This process was repeated until each of the k-folds served as the validation data set. The mean R^2 and RMSE values were used to assess the model accuracy. Finally, the model was applied to the test data set, and then the predictive ability was evaluated from the R^2, RMSE and RMSEr values.

3. Results

3.1. Plant height from field observations

The field PH of 167 accessions of upland rice was measured on 5 September 2018 (DAS 88) is shown in Figure 5, and Table 2 summarizes the minimum, maximum, median, mean, SD and coefficients of variation (CV) values. In theory, the accuracy of linear regression analysis is influenced by the SD and range of a sample, which is considered to be the reason why research on tall crops (e.g. barley, maize, sorghum) is prioritized. In the present study, our field PH data set covered a wide range of variations in plant 3D structure. The mean (and SD) value was 126.71 cm (±17.06 cm), with a range of 78.25–189.75 cm, and CV of 13.46%. The ANOVA results indicated that the effect of accession was statistically significant ($p < 0.001$) and its contribution ratio was estimated to be approximately 20% (Table 3). The remaining was accounted by error term, presumably because of large soil heterogeneity.

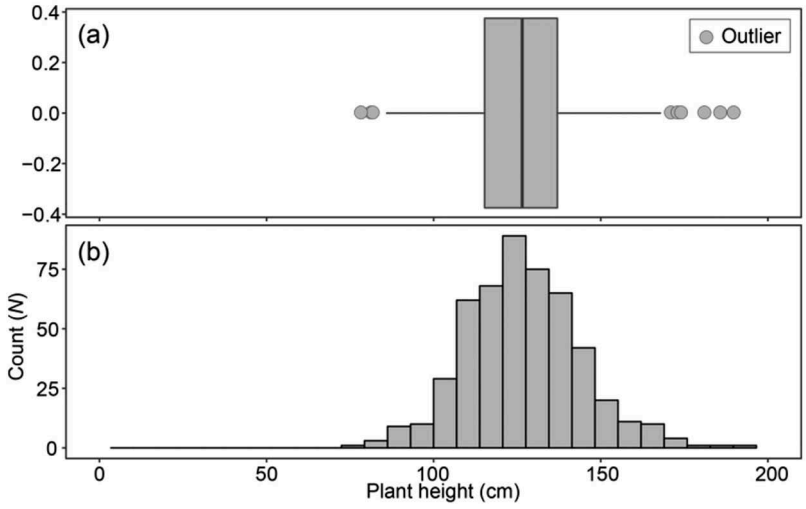

Figure 5. Box plot (a) and histogram (b) of the field PH on 5 September 2018 (DAS = 88).

Table 2. Descriptive statistics of field PH data. *n*, number of samples; SD, standard deviation; CV, coefficient of variation (SD/mean × 100%).

Data set	*n*	Min	Max	Median	Mean	SD	CV
PH (cm)	501	78.25	189.75	126.50	126.71	17.06	13.46

Table 3. Statistical results from ANOVA and percentage of contribution ratio by effects of accession, replication and error.

	Degree of freedom	Sum of square	Mean square	*F* ratio	Contribution rate (%)
Variety	158	65,487	414	1.77 ***	19.6
Rep	2	478	239	1.02 ns	0.0
Error	340	79,527	234		80.4
Total	500	145,492			

Contribution ratios for the effects of accession and replication were estimated by using Equation (2). The ratio for error term was calculated by subtracting the ratios of accession and replication from 100%.
***: $p < 0.001$
ns: not significant

3.2. Development of CHM from $DSMt_1$ and $DSMt_2$

Figure 6 shows the georeferenced orthomosaic RGB and DSM images for t_1 (12 June 2018) and t_2 (8 September 2018), and the CHM image of the upland rice field. The $DSMt_1$ values at emergence (no vegetation) ranged between 167.8 and 169.4 m, while the $DSMt_2$ values before the flowering stage ranged between 167.7 and 171.0 m.

The CHM in cm unit was developed from the $DSMt_2$-$DSMt_1$ difference based on the GSD 1 cm raster image (Figure 6(e)). To assess the vertical error, the CHM values at 6 GCPs (see Figure 2) were extracted. The mean value of the CHMs at GCPs was − 1.34 cm (standard deviation [SD] = 7.36 cm). In addition to PH data set, the CHM image also exhibited the large spatial variation and included '*among-plot*' variation as well '*within-plot*' variation.

3.3. CHMs-PH relationships

Relationships between field PH and CHM metrics of 90–99th percentiles (CHM90th to CHM99th) and top 1–10% values (CHM1% to CHM10%) are shown in Figure 7, and Table 4 summarizes the R^2, RMSE, RMSEr, intercept and slope of the regression line. Most of the CHM metrics had a significant correlation with field PH ($p < 0.001$), but they showed higher values than field PH. These biases became larger from the 99th percentile to the 90th percentile. Similar trends were obtained in the top 1–10% values of the CHM metrics, but the best R^2 and minimum RMSE values were obtained for the CHM metrics when CHM3% was used, and above CHM2%, the RMSE values were slightly increased.

3.4. Evaluation of the predictive ability

To evaluate the predictive ability of the CHM metrics, a 5-fold cross validation was conducted. Figure 8 shows the cross-validated mean RMSE values in the training/validation data (n = 400) from the 90–99th percentile and top 1–10% values in ROIs, and Table 5 summarizes the cross-validated mean R^2 and RMSE values in the validation data set and R^2, RMSE and RMSEr values from the model on the independent test data set (n = 101). Similar to the field PH-CHM relationship, the best mean R^2 (0.701) and minimum mean RMSE (9.264 cm) values in the cross validation were obtained for the CHM metrics when CHM3% was used. When the model was applied to the test data set,

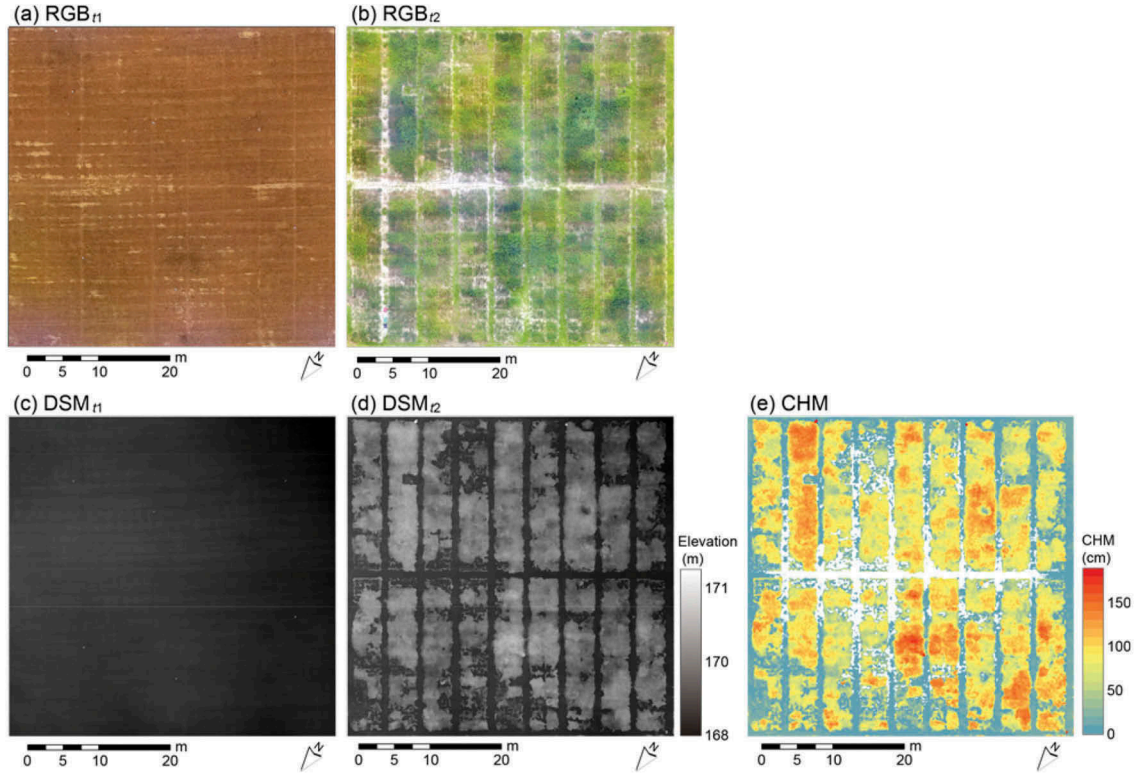

Figure 6. Orthomosaic-RGB images on June 12 (a) and September 8 (b) in 2018; DSMs at ground (c) and canopy levels (d), and CHM (e).

the best R^2 (0.780) and the minimum RMSE (8.823 cm) and RMSEr (6.963%) values were also obtained.

4. Discussion

This study investigated the potential of UAV platforms to use field-based phenotyping and focused especially on the PH as a case study for upland rice field in Laos. Our field PH data of 167 successions obtained before the flowering stage, indicated a wide variation in PH (78.25–189.75 cm) (Table 2). Previous research on upland rice fields reported that the field measured PH at the maturity stage ranged from 66 to 94 cm from nine genotypes in 10 environments in Luang Prabang province, Laos (Asai et al., 2009) or 66–126 cm from six cultivars under low or high soil fertilities in West Africa (Saito & Futakuchi, 2009). By comparison, our data set can be considered to have a wider range of variation in PH due to the great diversity of 167 accessions. A wide variation in data is essential to obtain a good correlation between the field PH and CHM metrics. The CHM in this study obtained from distance from two DTMs, so the vertical error was not so strongly depending on the GNSS accuracy, and the 10 cm error could be expected to use for the initial screenings in efficient way at the field.

The timing of UAV observation is also important for assessing PH. Previous studies in maize (Wang et al., 2019) and wheat (Holman et al., 2016) indicated that the PH varies greatly among different stages of development, and the correlation between the field PH and CHM increases with plant growth and PH. In contrast, the correlations are weaker in the early growth stages due to the limited range of variation of PH (Madec et al., 2017) and the lower canopy coverage because a higher proportion of pixels showing a lower level plant structure (Holman et al., 2016). To remove the effects, earlier studies generated CHM metrics from the 95th or 99th percentile rather than the standard mean or median because this method was best at isolating the top photosynthetic tissue of each plant and avoiding occasional contamination of individual rogue or anomalous plants.

However, even with CHM metrics from the 99th percentile, the proportion of the lower layer pixels may increase due to differences in plant structure depending on the successions of rice. Therefore, this study developed a CHM from the top 1–10% of the largest pixel values (CHM1% to CHM10%) for assessing PH and compared it with the CHM from the 90–99th percentiles (CHM90th to CHM99th). As we expected, CHM1–10% showed a better correlation (R^2 = 0.703–0.712, RMSE = 7.215–7.325 cm and RMSER = 7.215–7.325%) with field PH than CHM91–99th (R^2 = 0.678–0.708, RMSE = 9.201–9.675 cm, and RMSEr = 7.262–7.636%) (Table 4). The results in the 5-fold cross validation also showed a similar tendency, as

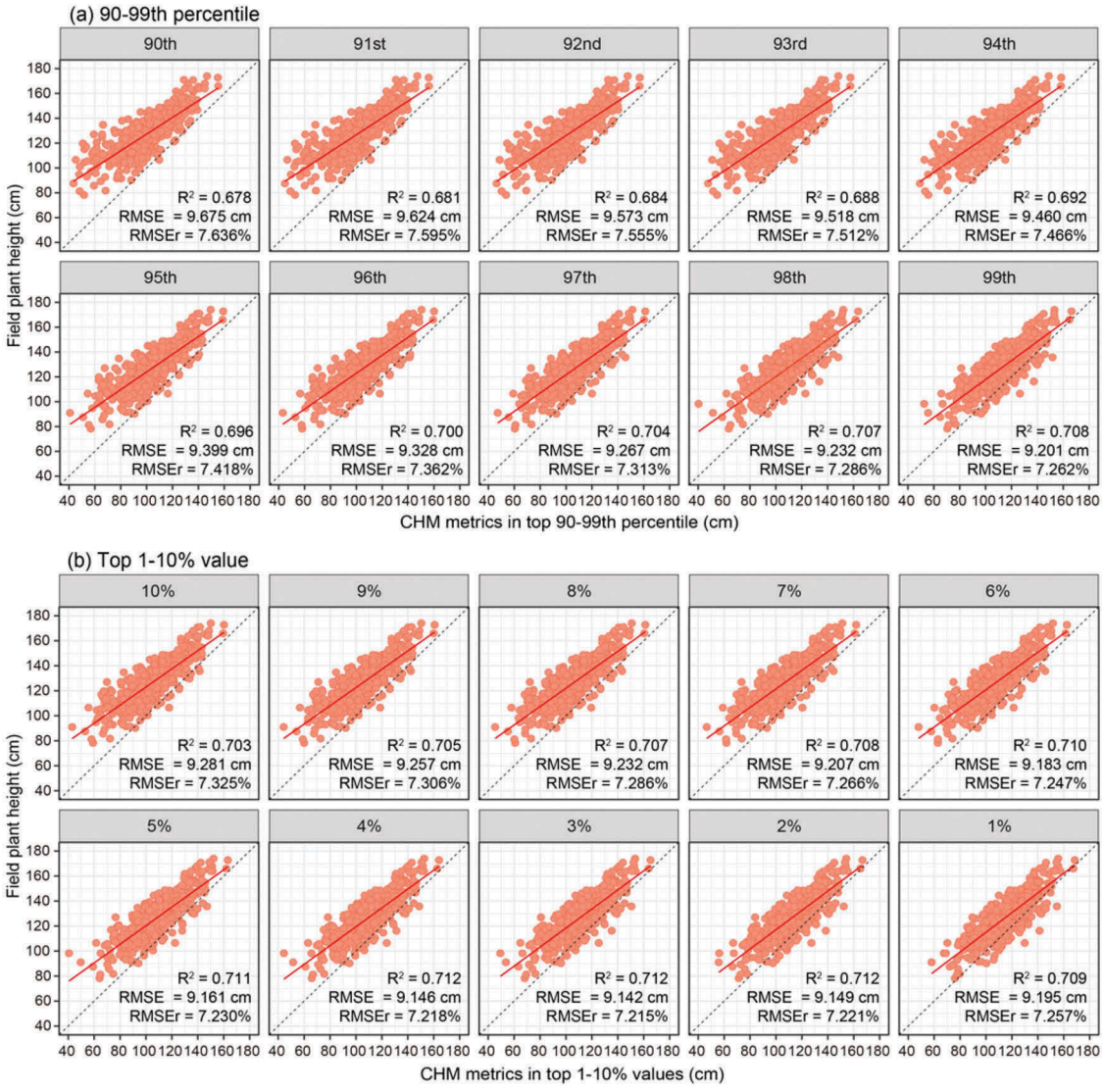

Figure 7. Relationships between field PH and CHM metrics of 90–99th percentiles (a) and top 1–10% of the largest values (a) in ROIs. The dashed line is the 1:1 line, and the red solid line is the regression line.

the cross-validated mean RMSE of CHM1–10% (R^2 = 0.692–0.701 and RMSE = 9.264–9.387 cm) overcame that of CHM90–99th (R^2 = 0.664–0.698 and RMSE = 9.322–9.772 cm) (Figure 8; Table 5). Overall, the best R^2 and minimum RMSE values were obtained by CHM3%, both in the correlation analysis and cross validation. These results indicated that the top 1–10% of the largest pixel values were a better approach to extract the CHM for assessing PH than the percentile values, and CHM3% would be optimal in the upland field.

In the present study, the 5-fold cross validation demonstrated that the field PH before flowering in upland rice can be estimated from CHM3% with a RMSE of 9.264 cm. When the model was applied for the test data set, the PH could be estimated with a RMSE of 8.823 cm (R^2 = 0.780), which represents a 6.963% error (RMSEr). Compared with a similar study by Shi et al. (2016) on maize (R^2 = 0.35) and sorghum (R^2 = 0.55) at the vegetative stage using CHM from multispectral camera image with 6.5 cm GSD at 122 m altitude, our results obtained better predictive accuracy for PH estimations using higher spatial resolution images (GSD 1 cm). Higher point cloud density and spatial resolution with lower flight level are critical to producing a high-quality CHM (Brocks et al., 2016). Moreover, the correlation between the field PH and CHM is varied due to the crop type and growth stage (Brocks & Bareth, 2018; Malambo et al., 2018). For example, the expected height before and after flowering changes from the leaf to ear (Han, Thomasson, Bagnall, Pugh et al., 2018). Malambo et al. (Malambo et al., 2018) reported that the correlation and RMSE values varied for maize (R^2 = 0.42–0.91, 11–18 cm) and sorghum (R^2 = 0.67–0.85, 12–22 cm) and found that the 99th percentile was generally more

Table 4. Coefficient of determination (R^2), root mean squared error (RMSE), relative RMSE (RMSE*r*), intercept and slope from regression analyses between field PH and CHM metrics.

CHM metrics	R^2	RMSE	RMSE*r*	Intercept	Slope
90–99th percentile					
90th	0.678	9.675	7.636	60.052	0.674
91st	0.681	9.624	7.595	58.767	0.681
92nd	0.684	9.573	7.555	57.363	0.689
93rd	0.688	9.518	7.512	55.874	0.698
94th	0.692	9.460	7.466	54.278	0.706
95th	0.696	9.399	7.418	52.464	0.716
96th	0.700	9.328	7.362	50.306	0.728
97th	0.704	9.267	7.313	47.679	0.741
98th	0.707	9.232	7.286	44.442	0.758
99th	0.708	9.201	7.262	39.748	0.780
Top 1–10%					
10%	0.703	9.281	7.325	50.073	0.731
9%	0.705	9.257	7.306	49.089	0.736
8%	0.707	9.232	7.286	48.028	0.742
7%	0.708	9.207	7.266	46.876	0.748
6%	0.710	9.183	7.247	45.601	0.754
5%	0.711	9.161	7.230	44.168	0.761
4%	0.712	9.146	7.218	42.528	0.769
3%	0.712	9.142	7.215	40.594	0.778
2%	0.712	9.149	7.221	38.178	0.788
1%	0.709	9.195	7.257	34.723	0.801

Table 5. Mean values of R^2 and RMSE from 5-fold cross validation using training/validation data sets based on a linear regression analysis and R^2, RMSE, and RMSEr based on the model applied to the test data sets.

	Validation data		Test data		
CHM metrics	Mean R^2	Mean RMSE	R^2	RMSE	RMSEr
90–99th percentile					
90th	0.664	9.772	0.761	9.347	7.377
91st	0.668	9.721	0.763	9.301	7.340
92nd	0.672	9.670	0.764	9.260	7.308
93rd	0.676	9.616	0.766	9.216	7.273
94th	0.680	9.559	0.768	9.167	7.235
95th	0.685	9.502	0.770	9.106	7.186
96th	0.689	9.437	0.773	9.028	7.125
97th	0.693	9.380	0.775	8.963	7.074
98th	0.695	9.364	0.780	8.863	6.995
99th	0.698	9.322	0.776	8.899	7.023
Top 1–10%					
10%	0.692	9.387	0.776	8.968	7.078
9%	0.693	9.364	0.776	8.948	7.062
8%	0.695	9.340	0.777	8.926	7.045
7%	0.697	9.316	0.778	8.903	7.027
6%	0.699	9.294	0.779	8.879	7.008
5%	0.700	9.276	0.780	8.855	6.988
4%	0.701	9.264	0.780	8.835	6.973
3%	0.701	9.264	0.780	8.823	6.963
2%	0.701	9.272	0.779	8.835	6.973
1%	0.697	9.309	0.775	8.923	7.042

strongly correlated with the field PH for maize while the 90th percentile was more strongly correlated with the field PH for sorghum. When even higher accuracy is required, terrestrial LiDAR is another option, although it is relatively expensive and has lower mobility. Previous studies have reported that ground LiDAR-based PH estimations achieved better accuracy than the UAV-CHM approach (Holman et al., 2016; Madec et al., 2017). For example, Holman et al. (Holman et al., 2016) reported that LiDAR biases in wheat are only 0.4 cm, which is low relative to that of UAV-CHM (2.4–15.8 cm error). Nevertheless, for practical use or first screening in breeding trials, the flexibility and affordability of UAV platforms and recent improvements to cameras will probably make UAVs the standard tool high-throughput field phenotyping of PH (Madec et al., 2017).

The CHM metrics in the present study showed a systematic overestimation compared with the field PH

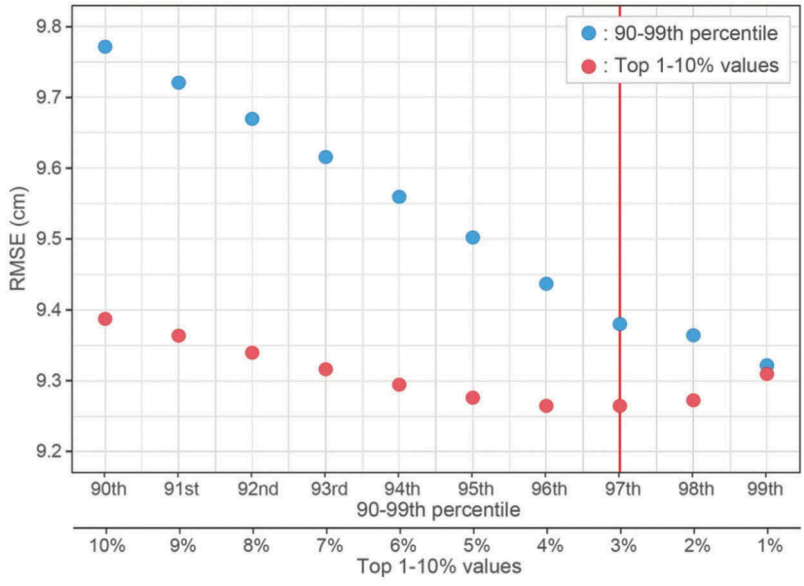

Figure 8. Changes in the mean RMSE values from the 5-fold cross validation in regression analyses between field PH and CHM height based on the 90–99th percentile (blue dots) and top 1–10% of the largest values (red dots) in ROIs. The red vertical line represents the minimum value of RMSE.

(Figure 7). This result is consistent with previous findings (Bareth et al., 2016; Grenzdörffer, 2014), indicating that the UAV-based SfM techniques lack the ability to accurately reconstruct the top of the canopy. Additionally, this result is partly affected by the spatial resolution compared to the size of the objects at the top of the canopy (Madec et al., 2017). Holman et al. (2016) also reported that the CHM underestimated wheat PH (2.4–15.8 cm error), with the lowest altitude imagery (highest spatial resolution) showing the lowest bias. In contrast, increasing the spatial resolution will lead to more noisy dense clouds with more gaps over plant coverage areas (Brocks et al., 2016; Madec et al., 2017). Moreover, Madec et al. (2017) indicated that a larger field of view with shorter focal lengths would generate more accurate 3D dense point clouds from SfM. Thus, better accuracy can be expected with optimal higher resolution images obtained at lower altitudes with adequate camera settings, although a trade-off occurs between accuracy and efficiency. While low-altitude UAV flights offer much higher image resolution, the ground coverage of an individual image is much smaller, which may result in inadequate coverage and insufficient overlap between images if a low flight speed cannot be maintained (Shi et al., 2016). The results of the present study were obtained at 20 m altitude (GSD 1 cm) in a small experimental field. For practical use by farmers, additional tests with different flight parameters to consider work efficiency are needed in the future.

Based on the CHM from UAV imagery, in this study, the PH was determined before the flowering stage, which is an almost mature stage that can be used to obtain data for a stable trait. CHMs can also be used for site-specific crop management (Schellberg et al., 2008; N. Zhang et al., 2002), plant nitrogen estimates (Eitel et al., 2014), and yield and biomass estimations (Bendig et al., 2015; Hoffmeister et al., 2016; Li et al., 2016). However, the best CHM metrics would vary according to the crop growth stage due to the difference of plant canopy structure (Brocks & Bareth, 2018; Malambo et al., 2018). Thus, in the present study, the single date measurements limit the monitoring of dynamic development and the relationship between plant growth and environmental variables, which form an important focus of next-generation phenotyping (Walter et al., 2015). Therefore, further analysis is needed for investigations using CHM metrics with multitemporal data sets collected during the growing season.

5. Conclusions

Low-cost small UAVs have great potential for rapid measurements of PH in crop fields. In this study, we used a small UAV for field-based phenotyping to estimate the PH in an upland rice field in Laos. Based on a comparative approach using 90–99 percentiles and top 1–10% values, our results indicated that PH was accurately estimated by CHM metrics of the top 3% pixel values with an 8.839 cm error, and the CHM3% was the best for assessing PH of whole canopy in a plot before flowering stage. The field data collection at 501 plots required more than 3 people × 1 day, while the UAV flight operation required only one person × 12 min. These results indicated that the CHM from a UAV platform can be used to estimate PH in a quick and cost-effective manner. Because genomics-assisted breeding studies require phenotyping of a large number of accessions or plants, our proposed method based on UAV remote sensing would be an important and valuable tool for high-throughput in-field phenotyping. Moreover, the dynamic development of rice plants could be assessed by multitemporal data sets. Future studies should obtain data sets through the growing season, examine the changes in PH and calculate the growth rate.

Acknowledgments

This study was conducted as part of a project sponsored by the Japan International Research Center for Agricultural Sciences (JIRCAS) on the "Multiple use and value addition of the regional resources for sustainable improvement of productivity in the semi-mountainous villages in Indo-china". We are grateful to Dr. Hiroshi Ikeura of the JIRCAS, Japan, for his valuable comments. We also thank Ms. Alisala Dethvongsa, Ms. Bownnou Tansoukhang and Mr. Chanpheng Xaymany of the Rice Research Center, NAFRI, Laos, for their support in the field experiments.

Disclosure statement

No potential conflict of interest was reported by the authors.

ORCID

Kensuke Kawamura http://orcid.org/0000-0002-2824-1266
Hidetoshi Asai http://orcid.org/0000-0003-0125-1234

References

Andrade-Sanchez, P., Gore, M. A., Heun, J. T., Thorp, K. R., Carmo-Silva, A. E., French, A. N., Salvucci, M. E., & White, J. W. (2013). Development and evaluation of a field-based high-throughput phenotyping platform. *Functional Plant Biology*, *41*(1), 68–79. https://doi.org/org/10.1071/FP13126

Appa Rao, S., Schiller, J.M., Bounphanousay, C., & Jackson, M. (2006). Chapter 9: Diversity within the traditional rice varieties of Laos. (Eds.) Schiller J.M., Chanphengxay, M.B., Linquist B., Appa Rao S., In Rice in Laos. Los Baños (Philipines) International Rice Research Institute, 457p.

Araus, J. L., & Cairns, J. E. (2014). Field high-throughput phenotyping: The new crop breeding frontier. *Trends in Plant Science*, *19* (1), 52–61. https://doi.org/10.1016/j.tplants.2013.09.008

Asai, H., Saito, K., Samson, B., Songyikhangsuthor, K., Homma, K., Shiraiwa, T., Kiyono, Y., Inoue, Y., & Horie, T. (2009). Yield response of indica and tropical japonica genotypes to soil fertility conditions under rainfed uplands in northern Laos. *Field Crops Research*, *112*(2–3), 141–148. https://doi.org/10.1016/j.fcr.2009.02.010

Asai, H., Soisouvanh, P., Sengxua, P., Kimura, K., Vongphuthine, B., & Ando, M. (2017). Labour-saving practices for the external expansion of Swidden agriculture for upland rice production in a mountainous area of Laos. *Tropical Agriculture and Development*, *61*(4), 166–178. https://doi.org/10.11248/jsta.61.166

Bareth, G., Bendig, J., Tilly, N., Hoffmeister, D., Aasen, H., & Bolten, A. (2016). A comparison of UAV- and TLS-derived plant height for crop monitoring: using polygon grids for the analysis of Crop Surface Models (CSMs). *Photogrammetrie - Fernerkundung - Geoinformation*, *2016* (2), 85–94. https://doi.org/10.1127/pfg/2016/0289

Bendig, J., Bolten, A., & Bareth, G. (2013). UAV-based Imaging for Multi-Temporal, very high Resolution Crop Surface Models to monitor Crop Growth VariabilityMonitoring des Pflanzenwachstums mit Hilfe multitemporaler und hoch auflösender Oberflächenmodelle von Getreidebeständen auf Basis von Bildern. *Photogrammetrie - Fernerkundung - Geoinformation*, *2013*(6), 551–562. https://doi.org/10.1127/1432-8364/2013/0200

Bendig, J., Bolten, A., Bennertz, S., Broscheit, J., Eichfuss, S., & Bareth, G. (2014). Estimating biomass of barley using crop surface models (CSMs) derived from UAV-based RGB imaging. *Remote Sensing*, *6*(11), 10395. https://doi.org/10.3390/rs61110395

Bendig, J., Yu, K., Aasen, H., Bolten, A., Bennertz, S., Broscheit, J., Gnyp, M. L., & Bareth, G. (2015). Combining UAV-based plant height from crop surface models, visible, and near infrared vegetation indices for biomass monitoring in barley. *International Journal of Applied Earth Observation and Geoinformation*, *39*, 79–87. https://doi.org/10.1016/j.jag.2015.02.012

Berni, J. A. J., Zarco-Tejada, P. J., Suárez, L., & Fereres, E. (2009). Thermal and narrowband multispectral remote sensing for vegetation monitoring from an unmanned aerial vehicle. *IEEE Transactions on Geoscience and Remote Sensing*, *47*(3), 722–738. https://doi.org/10.1109/TGRS.2008.2010457

Boomsma, C. R., Santini, J. B., West, T. D., Brewer, J. C., McIntyre, L. M., & Vyn, T. J. (2010). Maize grain yield responses to plant height variability resulting from crop rotation and tillage system in a long-term experiment. *Soil and Tillage Research*, *106*(2), 227–240. https://doi.org/10.1016/J.STILL.2009.12.006

Brocks, S., & Bareth, G. (2018). Estimating barley biomass with crop surface models from oblique RGB imagery. *Remote Sensing*, *10*(2), 268. https://doi.org/10.3390/rs10020268

Brocks, S., Bendig, J., & Bareth, G. (2016). Toward an automated low-cost three-dimensional crop surface monitoring system using oblique stereo imagery from consumer-grade smart cameras. *Journal of Applied Remote Sensing*, *10*(4), 046021. https://doi.org/10.1117/1.JRS.10.046021

Côté, J. F., Widlowski, J. L., Fournier, R. A., & Verstraete, M. M. (2009). The structural and radiative consistency of three-dimensional tree reconstructions from terrestrial lidar. *Remote Sensing of Environment*, *113*(5), 1067–1081. https://doi.org/10.1016/j.rse.2009.01.017

De Souza, C. H. W., Lamparelli, R. A. C., Rocha, J. V., & Magalhães, P. S. G. (2017). Height estimation of sugarcane using an unmanned aerial system (UAS) based on structure from motion (SfM) point clouds. *International Journal of Remote Sensing*, *38*(8–10), 2218–2230. https://doi.org/10.1080/01431161.2017.1285082

Eitel, J. U. H., Magney, T. S., Vierling, L. A., Brown, T. T., & Huggins, D. R. (2014). LiDAR based biomass and crop nitrogen estimates for rapid, non-destructive assessment of wheat nitrogen status. *Field Crops Research*, *159*, 21–32. https://doi.org/10.1016/j.fcr.2014.01.008

Emmert-Streib, F., & Dehmer, M. (2019). Evaluation of regression models: Model assessment, model selection and generalization error. *Machine Learning and Knowledge Extraction*, *1*(1), 521–551. https://doi.org/10.3390/make1010032

Fahlgren, N., Gehan, M. A., & Baxter, I. (2015). Lights, camera, action: High-throughput plant phenotyping is ready for a close-up. *Current Opinion in Plant Biology*, *24*, 93–99. https://doi.org/10.1016/j.pbi.2015.02.006

Furbank, R. T., & Tester, M. (2011). Phenomics - technologies to relieve the phenotyping bottleneck. *Trends in Plant Science*, *16*(12), 635–644. https://doi.org/10.1016/j.tplants.2011.09.005

Grenzdörffer, G. J. (2014).Crop height determination with UAS point clouds. In *International archives of the photogrammetry, remote sensing and spatial information sciences - ISPRS archives* (Vol. 40, pp. 135–140) International Society for Photogrammetry and Remote Sensing (ISPRS). https://doi.org/10.5194/isprsarchives-XL-1-135-2014

Großkinsky, D. K., Svensgaard, J., Christensen, S., & Roitsch, T. (2015). Plant phenomics and the need for physiological phenotyping across scales to narrow the genotype-to-phenotype knowledge gap. *Journal of Experimental Botany*, *66*(18), 5429–5440. https://doi.org/10.1093/jxb/erv345

Han, X., Thomasson, J. A., Bagnall, C., Rooney, W. L., Pugh, N. A., Horne, D. W., Rooney, W. L., Malambo, L., Chang, A., Jung, J., & Cope, D. A. (2018). Calibrated plant height estimates with structure from motion from fixed-wing UAV images. Proceedings of the Society of Photo-Optical Instrumentation Engineers (SPIE) 10664, *Autonomous Air and Ground Sensing Systems for Agricultural Optimization and Phenotyping III*, 106640D. https://doi.org/10.1117/12.2305746

Han, X., Thomasson, J. A., Bagnall, G. C., Pugh, N. A., Horne, D. W., Rooney, W. L., Jung, J., Chang, A., Malambo, L., Popescu, S. C., Gates, I. T., & Cope, D. A. (2018). Measurement and calibration of plant-height from fixed-wing UAV images. *Sensors (Basel, Switzerland)*, *18*(12), 4092. https://doi.org/10.3390/s18124092

Hijmans, R. J. (2019). raster: geographic data analysis and modeling. R package version 2.9-5. https://CRAN.R-project.org/package=raster

Hoffmeister, D., Waldhoff, G., Korres, W., Curdt, C., & Bareth, G. (2016). Crop height variability detection in a single field by multi-temporal terrestrial laser scanning. *Precision Agriculture*, *17*(3), 296–312. https://doi.org/10.1007/s11119-015-9420-y

Holman, F. H., Riche, A. B., Michalski, A., Castle, M., Wooster, M. J., & Hawkesford, M. J. (2016). High throughput field phenotyping of wheat plant height and growth rate in

field plot trials using UAV based remote sensing. *Remote Sensing*, *8*(12), 1031. https://doi.org/10.3390/rs8121031

Hu, P., Chapman, S. C., Wang, X., Potgieter, A., Duan, T., Jordan, D., Guo, Y., & Zheng, B. (2018). Estimation of plant height using a high throughput phenotyping platform based on unmanned aerial vehicle and self-calibration: Example for sorghum breeding. *European Journal of Agronomy*, *95*, 24–32. https://doi.org/10.1016/j.eja.2018.02.004

Hunt, E. R., Hively, W. D., Fujikawa, S., Linden, D., Daughtry, C. S., & McCarty, G. (2010). Acquisition of NIR-green-blue digital photographs from unmanned aircraft for crop monitoring. *Remote Sensing*, *2*(1), 290–305. https://doi.org/10.3390/rs2010290

James, M. R., & Robson, S. (2014). Mitigating systematic error in topographic models derived from UAV and ground-based image networks. *Earth Surface Processes and Landforms*, *39* (10), 1413–1420. https://doi.org/10.1002/esp.3609

Korhonen, L., Korpela, I., Heiskanen, J., & Maltamo, M. (2011). Airborne discrete-return LIDAR data in the estimation of vertical canopy cover, angular canopy closure and leaf area index. *Remote Sensing of Environment*, *115*(4), 1065–1080. https://doi.org/10.1016/j.rse.2010.12.011

Li, W., Niu, Z., Chen, H., Li, D., Wu, M., & Zhao, W. (2016). Remote estimation of canopy height and aboveground biomass of maize using high-resolution stereo images from a low-cost unmanned aerial vehicle system. *Ecological Indicators*, *67*, 637–648. https://doi.org/10.1016/j.ecolind.2016.03.036

Madec, S., Baret, F., De Solan, B., Thomas, S., Dutartre, D., Jezequel, S., Hemmeré, M., Colombeau, G., & Comar, A. (2017). High-throughput phenotyping of plant height: Comparing unmanned aerial vehicles and ground LiDAR estimates. *Frontiers in Plant Science*, *8*, 2002. https://doi.org/10.3389/fpls.2017.02002

Malambo, L., Popescu, S. C., Murray, S. C., Putman, E., Pugh, N. A., Horne, D. W., Richardson, G., Sheridan, R., Rooney, W. L., Avant, R., Vidrine, M., McCutchen, B., Baltensperger, D., & Bishop, M. (2018). Multitemporal field-based plant height estimation using 3D point clouds generated from small unmanned aerial systems high-resolution imagery. *International Journal of Applied Earth Observation and Geoinformation*, *64*, 31–42. https://doi.org/10.1016/j.jag.2017.08.014

Nebiker, S., Annen, A., Scherrer, M., & Oesch, D. (2008). A light-weight multispectral sensor for micro UAV – Opportunities for very high resolution airborne remote sensing. *XXI ISPRS Congress*, *XXXVII*(Part B1), 1194–1199. https://www.isprs.org/proceedings/XXXVII/congress/1_pdf/204.pdf

R Core Team. (2018). *R: A language and environment for statistical computing*. R Foundation for Statistical Computing. R Foundation for Statistical Computing. https://doi.org/10.1007/978-3-540-74686-7

Rosnell, T., & Honkavaara, E. (2012). Point cloud generation from aerial image data acquired by a quadrocopter type micro unmanned aerial vehicle and a digital still camera. *Sensors*, *12*(1), 453–480. https://doi.org/10.3390/s120100453

Rueda-Ayala, V. P., Peña, J. M., Höglind, M., Bengochea-Guevara, J. M., & Andújar, D. (2019). Comparing UAV-based technologies and RGB-D reconstruction methods for plant height and biomass monitoring on grass ley. *Sensors (Switzerland)*, *19*(3), 535. https://doi.org/10.3390/s19030535

Saito, K., Asai, H., Zhao, D., Laborte, A. G., & Grenier, C. (2018). Progress in varietal improvement for increasing upland rice productivity in the tropics. *Plant Production Science*, *21*(3), 145–158. https://doi.org/10.1080/1343943X.2018.1459751

Saito, K., & Futakuchi, K. (2009). Performance of diverse upland rice cultivars in low and high soil fertility conditions in West Africa. *Field Crops Research*, *111*(3), 243–250. https://doi.org/10.1016/j.fcr.2008.12.011

Salas Fernandez, M. G., Becraft, P. W., Yin, Y., & Lübberstedt, T. (2009). From dwarves to giants? Plant height manipulation for biomass yield. *Trends in Plant Science*, *14*(8), 454–461. https://doi.org/10.1016/j.tplants.2009.06.005

Sankaran, S., Khot, L. R., Espinoza, C. Z., Jarolmasjed, S., Sathuvalli, V. R., Vandemark, G. J., Miklas, P. N., Carter, A. H., Pumphrey, M. O., Knowles, N. R., & Pavek, M. J. (2015). Low-altitude, high-resolution aerial imaging systems for row and field crop phenotyping: A review. *European Journal of Agronomy*, *70*, 112–123. https://doi.org/10.1016/j.eja.2015.07.004

Schellberg, J., Hill, M. J., Gerhards, R., Rothmund, M., & Braun, M. (2008). Precision agriculture on grassland: Applications, perspectives and constraints. *European Journal of Agronomy*, *29* (2–3), 59–71. https://doi.org/10.1016/j.eja.2008.05.005

Shi, Y., Thomasson, J. A., Murray, S. C., Pugh, N. A., Rooney, W. L., Shafian, S., Yang, C., Morgan, C. L. S., Neely, H. L., Rana, A., Bagavathiannan, M. V., Henrickson, J., Bowden, E., Valasek, J., Olsenholler, J., Bishop, M. P., Sheridan, R., Putman, E. B., Popescu, S., Zhang, J., & Rajan, N. (2016). Unmanned Aerial vehicles for high-throughput phenotyping and agronomic research. *PloS One*, *11*(7), e0159781. https://doi.org/10.1371/journal.pone.0159781

Snavely, N., Seitz, S. M., & Szeliski, R. (2008). Modeling the world from Internet photo collections. *International Journal of Computer Vision*, *80*(2), 189–210. https://doi.org/10.1007/s11263-007-0107-3

Stavrakoudis, D., Katsantonis, D., Kadoglidou, K., Kalaitzidis, A., & Gitas, I. Z. (2019). Estimating rice agronomic traits using drone-collected multispectral imagery. *Remote Sensing*, *11* (5), 545. https://doi.org/10.3390/rs11050545

Van Iersel, W., Straatsma, M., Addink, E., & Middelkoop, H. (2018). Monitoring height and greenness of non-woody floodplain vegetation with UAV time series. *ISPRS Journal of Photogrammetry and Remote Sensing*, *141*, 112–123. https://doi.org/10.1016/j.isprsjprs.2018.04.011

Walter, A., Liebisch, F., & Hund, A. (2015). Plant phenotyping: From bean weighing to image analysis. *Plant Methods*, *11*(1), 14. https://doi.org/10.1186/s13007-015-0056-8

Wang, X., Zhang, R., Song, W., Han, L., Liu, X., Sun, X., Luo, M., Chen, K., Zhang, Y., Yang, H., Yang, G., Zhao, Y., & Zhao, J. (2019). Dynamic plant height QTL revealed in maize through remote sensing phenotyping using a high-throughput unmanned aerial vehicle (UAV). *Scientific Reports*, *9*(1), 3458. https://doi.org/10.1038/s41598-019-39448-z

Watanabe, K., Guo, W., Arai, K., Takanashi, H., Kajiya-Kanegae, H., Kobayashi, M., Yano, K., Tokunaga, T., Fujiwara, T., Tsutsumi, N., & Iwata, H. (2017). High-throughput phenotyping of sorghum plant height using an unmanned aerial vehicle and its application to genomic prediction modeling. *Frontiers in Plant Science*, *8*, 421. https://doi.org/10.3389/fpls.2017.00421

Westoby, M. J., Brasington, J., Glasser, N. F., Hambrey, M. J., & Reynolds, J. M. (2012). 'Structure-from-Motion'

photogrammetry: A low-cost, effective tool for geoscience applications. *Geomorphology*, *179*, 300–314. https://doi.org/10.1016/j.geomorph.2012.08.021

Zhang, C., & Kovacs, J. M. (2012). The application of small unmanned aerial systems for precision agriculture: A review. *Precision Agriculture*, *13*(6), 693–712. https://doi.org/10.1007/s11119-012-9274-5

Zhang, H., Sun, Y., Chang, L., Qin, Y., Chen, J., Qin, Y., Du, J., Yi, S., & Wang, Y. (2018). Estimation of grassland canopy height and aboveground biomass at the quadrat scale using unmanned aerial vehicle. *Remote Sensing*, *10*(6), 851. https://doi.org/10.3390/rs10060851

Zhang, L., & Grift, T. E. (2012). A LIDAR-based crop height measurement system for Miscanthus giganteus. *Computers and Electronics in Agriculture*, *85*, 70–76. https://doi.org/10.1016/j.compag.2012.04.001

Zhang, N., Wang, M., & Wang, N. (2002). Precision agriculture—a worldwide overview. *Computers and Electronics in Agriculture*, *36*(2–3), 113–132. https://doi.org/10.1016/s0168-1699(02)00096-0

Zhang, W., Wan, P., Wang, T., Cai, S., Chen, Y., Jin, X., & Yan, G. (2019). A novel approach for the detection of standing tree stems from plot-level terrestrial laser scanning data. *Remote Sensing*, *11*(2), 211. https://doi.org/10.3390/rs11020211